polyplex micelles prepared at N/P = 1.2 were used for further investigations.

The transfection efficiency and cytotoxicity of the polyplex micelles co-incubated with the DPc-incorporated micelles in the presence or absence of light irradiation (fluence: 5.4 J/cm^2) are shown in Figure 5(A) and (B), respectively. The same experimental procedures as in Figure 4 were applied in this study. Based on these results, the PCI using the DPc-incorporated micelles achieved a 56–212-fold photochemical enhancement of the transfection of the polyplex micelles while maintaining an approximately 80% cell viability over a wide range of DPc concentrations (0.4×10^{-7}–3.2×10^{-7} M) and showed an approximately 50% decrease in viability above the critical DPc concentration (6.4×10^{-7} M). Note that a similar photochemical enhancement of the transfection was observed when 293 T cells were used (data not shown). The maximal transfection level achieved by the PCI using the DPc-incorporated micelles was comparable to that obtained using hydroxychloroquine (hc), which has been demonstrated to be a potent endosomotropic agent (Itaka et al. 2004) (Figure 5(A)). Interestingly, the transfection efficiency of the polyplex micelles decreased as the concentration of the DPc-incorporated micelles increased, particularly under non-irradiated conditions (Figures 5(A) and 6(A)), thus leading to a remarkably high light-selectivity of the gene transfection. Such a DPc concentration-dependent decrease in the transfection efficiency of the polyplex micelles was not observed in the PCI using DPc alone (Figure 7(A)). There may be two possible explanations for this observation. First, the polyplex micelles may compete with the DPc-incorporated micelles in the cellular uptake due to similar particle sizes and surface properties. In Figure 5(A), the molar concentration of the DPc-incorporated micelles was estimated to be comparable to or 20-fold higher than that of the polyplex micelles at the DPc concentration of 2.0×10^{-8} or 6.4×10^{-7} M, respectively. An increase in the DPc concentration decreases the molar ratio of the pDNA-incorporated micelles to the DPc-incorporated micelles in the medium, leading to a decreased cellular uptake of the pDNA-incorporated micelles. Alternatively, the pDNA- and DPc-incorporated micelles may interact each other, thereby decreasing the transfection efficiency. Indeed, we observed in Figure 4(A) that an excess of PEG–PLL could decrease the transfection efficiency of the polyplex micelles in the PCI-mediated transfcetion. These possibilities may also account for the DPc concentration-dependent decrease in the transfection efficiency.

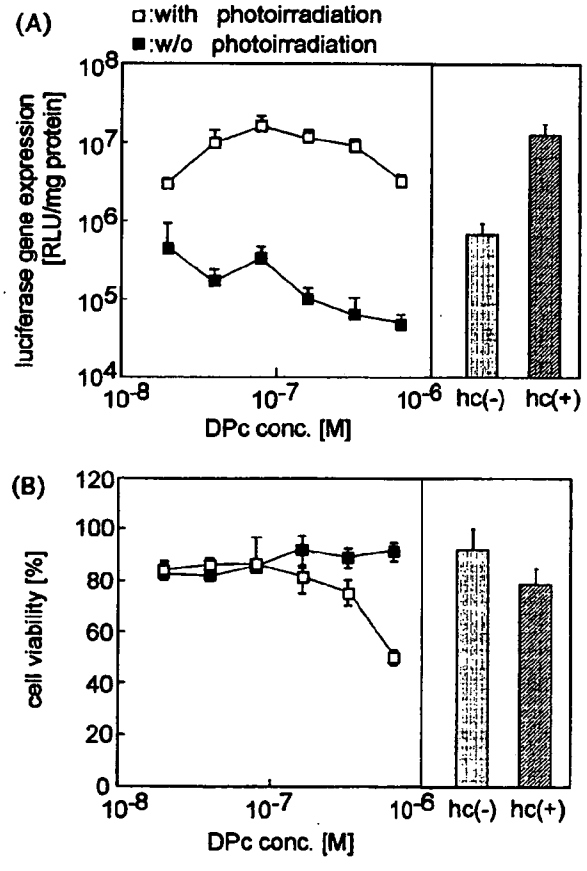

Figure 5. The effect of the DPc concentration on the transfection efficiency (A) and photocytotoxicity (B) in the PCI-mediated transfection using the DPc-incorporated micelles. The light irradiation (fluence: 5.4 J/cm^2) was performed 6 h after incubation with the pDNA- and DPc-incorporated micelles, followed by 48 h post-incubation in a fresh medium.

Regarding changes in cell viability in Figure 5(B), a DPc concentration-dependent decrease in cell viability was observed at the DPc concentrations above 1.6×10^{-7} M, while a DPc concentration-independent 10–20% decrease in cell viability was observed below 1.6×10^{-7} M DPc, regardless of photoirradiation. It is assumed that the DPc concentration-dependent decrease in cell viability observed at the region of high-DPc concentration might be attributable to the photochemical reactions in the PCI-mediated transfection. On the other hand, the 10–20% decrease in cell viability at the lower DPc concentration even without photoirradiation may be inducible by the DPc-incorporated micelles, since the pDNA-incorporated micelles alone did not show an appreciable cytotoxicity (Figures 6(C) and 7(C)). Nevertheless, such a 10–20% decrease in cell viability, of which the mechanisms remain to be clarified yet, is still in a tolerable range and is unlikely to be the serious limitations of this strategy.

The effects of the DPc concentration and fluence on the transfection efficiency of the polyplex micelles, photochemical enhancement of the transfection and photocytotoxicity in the PCI using the DPc-incorporated micelles were completely examined and the results are shown in Figure 6(A)–(C), respectively. Similarly, the PCI-mediated transfection of the pDNA/PEG–PLL polyplex micelles was carried out

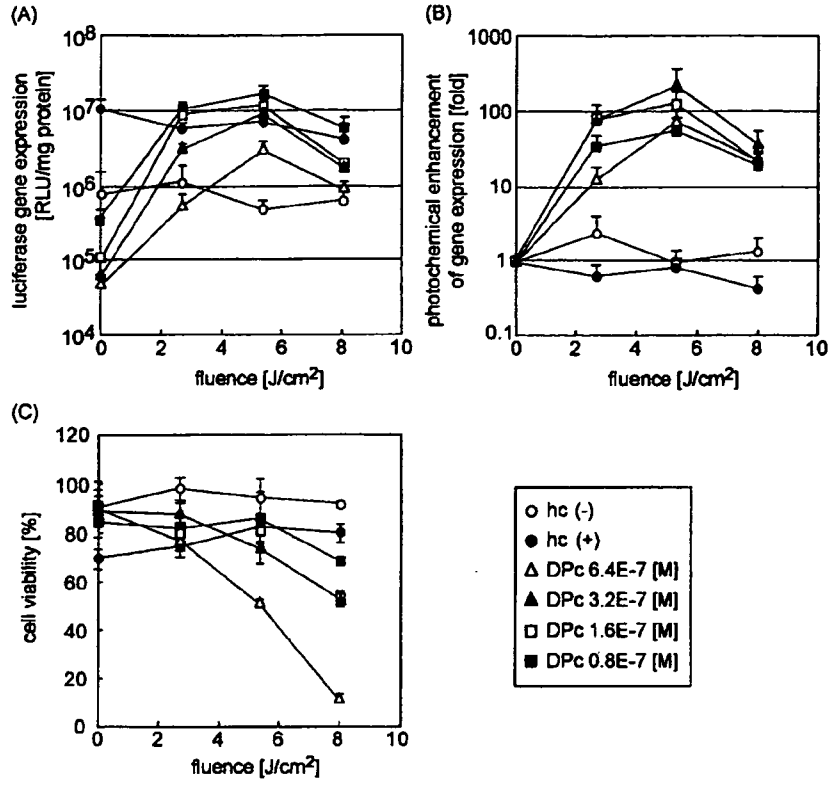

Figure 6. The effects on the DPc concentration and fluence on the transfection efficiency (A), photochemical enhancement of the gene expression (B) and photocytotoxicity (C) in the PCI-mediated transfection using the DPc-incorporated micelles. The light irradiation was performed 6 h after incubation with the pDNA- and DPc-incorporated micelles, followed by 48 h post-incubation in a fresh medium. The "hc" strands for hydroxychloroquine.

using DPc alone or $AlPcS_{2a}$, which was demonstrated to be an effective photosensitizer in the PCI (Høgset et al. 2002, 2004). These results are shown in Figures 7 and 8, respectively. Also, to easily compare the main differences between the results in Figures 6–8, the effects of each photosensitizer on the photochemical enhancement of the gene expression and cell viability at the fluence of 5.4 J/cm^2 are summarized in Table I. In the PCI using DPc alone, the highest transfection efficiency of the polyplex micelles was obtained with a 25–50% reduced cell viability (Figure 7(A) and (C)). The PCI using $AlPcS_{2a}$ showed a transfection activity comparable to that using the DPc-incorporated micelles; however, the photochemical enhancement of the transgene expression was accompanied by an inevitable photocytotoxicity (Figure 8(A) and (C)). Eventually, the PCI using the combination of the pDNA- and DPc-incorporated micelles showed the highest photochemical enhancement of the gene transfection of the polyplex micelles (Figure 6(B)), which may be attributed to the reduced transfection efficiency at comparatively high-concentrations of the DPc-incorporated micelles under non-irradiated conditions as discussed above as well as actual increases in the transfection efficiency. Such a high-light-selectivity of the gene transfection might be advantageous for accomplishing the site-directed gene transfer using the PCI concept. More importantly, the PCI using the DPc-incorporated micelles showed an appreciably wide range of safe DPc concentrations and light doses, in which a remarkable enhancement of the transfection was achieved without a substantial decrease in the cell viability (Figure 6(B) and (C)). The efficacy of this system was prominent even when compared with those of other systems using DPc alone and $AlPcS_{2a}$ as shown in Table I.

To achieve a systemic PCI-mediated gene delivery utilizing micellar nanocarriers, polymeric micelles are required to accumulate in the target tissues and be taken up by the target cells, of which processes are known to occur in a time-dependent manner. On the other hand, the timing of the photoirradiation may be a critical factor in the PCI-mediated transfection (Prasmickaite et al. 2001). Hence, the effect of the photoirradiation timing on the photochemical transfection was then investigated. First, the effect of the prolonged incubation before photoirradiation was examined: after a 24 h continuous incubation with the combination of the pDNA- and DPc-incorporated micelles, HeLa cells were subjected to the medium replacement, followed by photoirradiation at the fluence of 5.4 J/cm^2. The transfection efficacy was evaluated after a further 48 h of post-incubation. As seen in Figure 9, an approximately 50-fold photochemical enhancement in the gene expression while

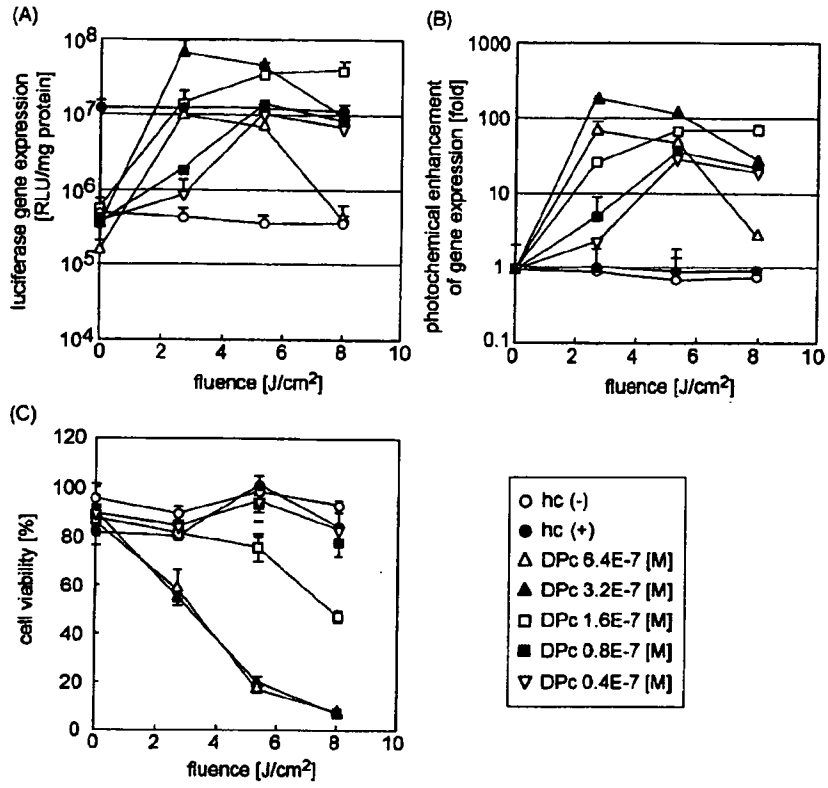

Figure 7. The effects on the DPc concentration and fluence on the transfection efficiency (A), photochemical enhancement of the gene expression (B) and photocytotoxicity (C) in the PCI-mediated transfection using DPc alone. The light irradiation was performed 6 h after incubation with the pDNA-incorporated micelles and free DPc, followed by 48 h post-incubation in a fresh medium.

maintaining more than an 80% cell viability was obtained under this condition, which appears to be consistent with Figure 5. Thus, the PCI using the DPc-incorporated micelles might be effective even after a prolonged incubation before photoirradiation. Note that the transfection efficiencies of the polyplex micelles under both irradiated and non-irradiated conditions decreased as the DPc concentration increased (Figure 9(A)), which may be due to the decreased cellular uptake of the polyplex micelles and/or interaction between the pDNA- and DPc-incorporated micelles as discussed above. In a second set of experiments, a certain lag time was placed before the photoirradiation of the HeLa cells in freshly replaced medium after a 6 h incubation with the combinational formulation of pDNA- and DPc-incorporated micelles. The transfection efficacy was evaluated 48 h after the photoirradiation (5.4 J/cm^2). As shown in Figure 10, post-incubation in the micelle-free medium after the 6 h treatment with the combinational micellar formulation resulted in a time-dependent decrease in the efficacy of the PCI-mediated transfection. This result seems to be consistent with the previous observation by Prasmickaite et al. (2001) suggesting that, in the PCI-mediated transfection, gene carriers may need to be translocated into the cytosol before their movement from the endosome to the lysosome. Therefore, to achieve a successful *in vivo* PCI-mediated gene delivery, the timing of the photoirradiation should be optimized in consideration of the balance between the effective accumulation of gene carriers as well as photosensitizers in the target cells and the prompt photo-induced translocation of gene carriers from the endosome to the cytosol before their movement to the lysosome.

The PCI is a smart concept, which can be basically used for the site-directed transfection in a light-inducible manner. In previous studies, $AlPcS_{2a}$ was demonstrated to be effective in the PCI (Høgset et al. 2002, 2004); however, the photochemical enhancement of the transfection was accompanied by the photocytotoxicity (Høgset et al. 2000). Although $AlPcS_{2a}$ is known to be internalized by the endocytic pathway, it is likely that $AlPcS_{2a}$ may interact with the plasma membrane to some extent as well as relocalize to some cytoplasmic organelles such as the mitochondria and endoplasmic reticulum during the photoirradiation, thereby inducing the inevitable photocytotoxicity (Moan et al. 1994; Macdonald and Dougherty 2001). Hence, considerable efforts have been devoted to the optimization of the experimental conditions for reducing the photocytotoxicity in the PCI-mediated transfection (Høgset et al. 2000). Also, the delivery of photosensitizers to the target cell should be taken into consideration in order to accomplish the *in vivo* PCI-mediated gene delivery.

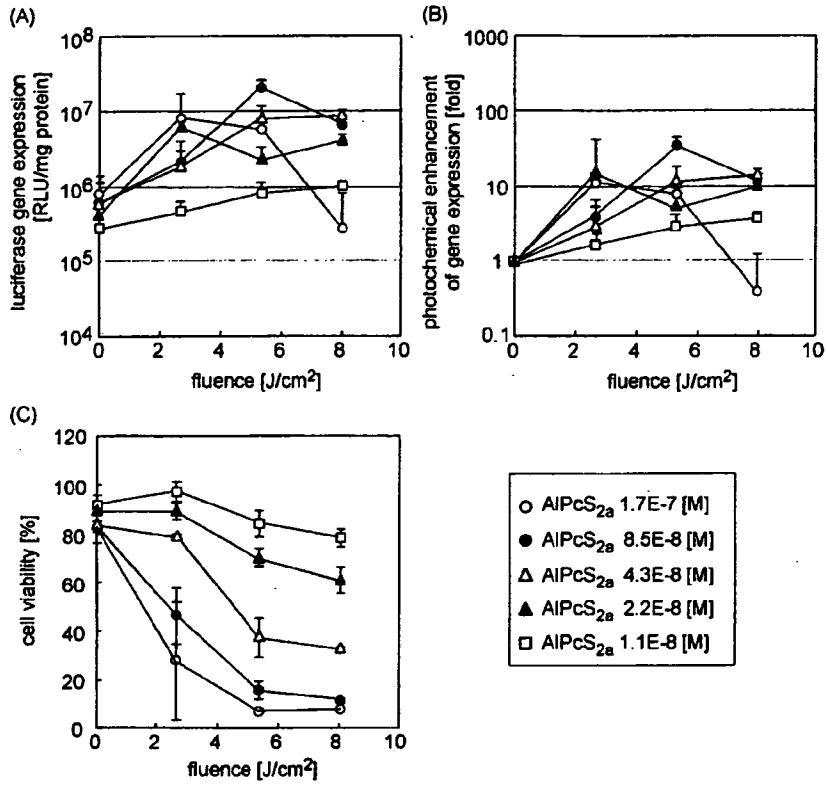

Figure 8. The effects on the $AlPcS_{2a}$ concentration and fluence on the transfection efficiency (A), photochemical enhancement of the gene expression (B) and photocytotoxicity (C) in the PCI-mediated transfection using $AlPcS_{2a}$. The light irradiation was performed 6 h after incubation with the pDNA-incorporated micelles and $AlPcS_{2a}$, followed by 48 h post-incubation in a fresh medium.

In this regard, we have recently developed DPc as a new photosensitizer for the PCI (Nishiyama et al. 2005). It has been demonstrated that the anionic DPc might electrostatically interact with the surface of the cationic polyplex to form the ternary complex enveloped with DPc, thus giving the same internalization and subcellular localization between DPc and the polyplex. Meanwhile, DPc exhibited a pH-dependent membrane binding ability, allowing the selective photodamaging of the endosomal membrane. Consequently, the ternary complex showed more than 100-fold photochemical enhancement of the gene expression with reduced photocytotoxicity on the cultured cells and *in vivo* light-selective gene transfer to the conjunctival tissues in rat eyes (Nishiyama et al. 2005). Thus, it was suggested that the design of the ternary complex might be effective for the PCI-mediated gene delivery; however, the ternary complex system is unlikely to be used for the systemic delivery. It is known that highly negatively-charged macromolecules can be excluded from the blood circulation due to the hepatic uptake by scavenger receptors of the non-parenchymal cells (Takakura and Hashida 1996).

In this study, the combinational formulation of the pDNA- and DPc-incorporated micelles was used in the PCI-mediated transfection. Polymeric micelles, of which the drug-loaded core is covered with a dense and hydrophilic PEG palisade, are characterized by their small size (less than 100 nm), excellent biocompatibility and stability in biological media (Kataoka et al. 1993, 2001; Nishiyama and Kataoka, 2006). We have so far demonstrated that polymeric micelles incorporating antitumor drugs can stably circulate in the bloodstream and effectively accumulate in solid tumors (Kwon et al. 1994; Nishiyama et al. 2003; Bae et al. 2005). Accordingly, in this study, we have used polymeric micelles as nanocarriers for the pDNA and DPc delivery, expecting their future application in systemic administration. In particular, this paper focused on demonstrating the feasibility of our strategy using the combinational formulation of the pDNA- and DPc-incorporated micelles in the PCI-mediated transfection *in vitro*. In this strategy, both polymeric micelles are assumed to be taken up by the cell through the endocytic pathway and show the same subcellular localization, allowing selective photochemical damaging of the endosomal membrane and effective cytoplasmic delivery of the pDNA-incorporated micelles upon photoirradiation, which might be a key to the successful PCI-mediated transfection. Indeed, the PCI using the DPc-incorporated micelles achieved more than 200-fold photochemical enhancement of the gene transfection of the polyplex micelles. Importantly, the PCI using the combinational micellar formulation achieved a wide range of safe DPc

Table I. Photochemical enhancement of the gene expression and cell viability in the PCI-mediated transfection using each photosensitizer (fluence: 5.4 J/cm^2).

DPc-loaded micelle	DPc conc. (μM)	0.64	0.32	0.16	0.08
	(a) Photochemical enhancement (fold)	72.6 ± 30	211 ± 150*	123 ± 58***	55.7 ± 25
	(b) Cell viability (%)	50.7 ± 1.9	73.8 ± 6.4**	81.2 ± 4.8	86.1 ± 11
DPc	DPc conc. (μM)	0.64	0.32	0.16	0.08
	(a) Photochemical enhancement (fold)	47.1 ± 20	117 ± 16**	64.3 ± 13***	34.2 ± 4.5
	(b) Cell viability (%)	15.7 ± 2.0	18.0 ± 2.3**	73.8 ± 5.8	92.0 ± 4.0
$AlPcS_{2a}$	$AlPcS_{2a}$ conc. (μM)	0.17	0.085	0.043	0.022
	(a) Photochemical enhancement (fold)	8.09 ± 8.9	35.5 ± 8.9*, **	12.9 ± 6.0***	5.63 ± 2.8
	(b) Cell viability (%)	7.15 ± 1.0	15.9 ± 3.7**	37.8 ± 7.8	71.4 ± 3.8

*$P > 0.05$; **$P < 0.01$; and ***$P < 0.05$ ($n = 4$, unpaired t-test).

concentrations and light doses, in which remarkable enhancement of the transfection was achieved without a significant decrease in the cell viability. Such expanded ranges of safe DPc concentrations and light doses should be favorable for the *in vivo* PCI-mediated gene delivery.

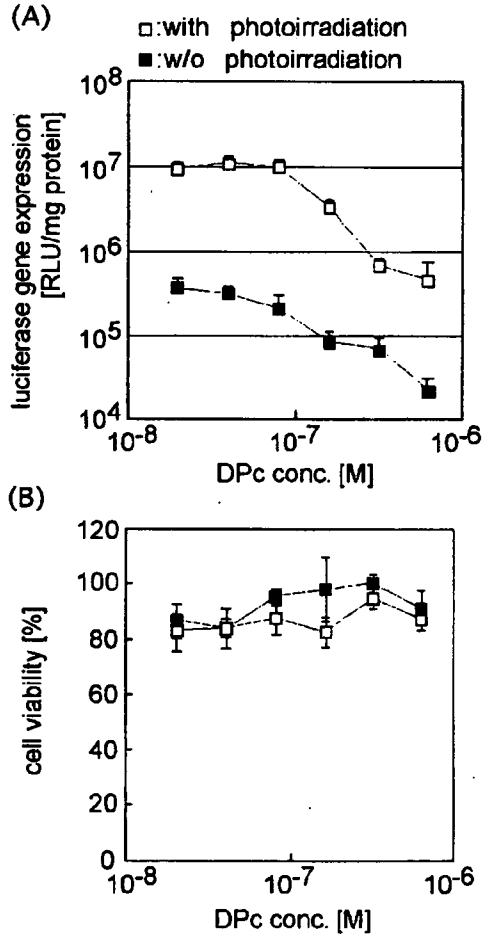

Figure 9. The transfection efficiency (A) and photocytotoxicity (B) in the PCI-mediated transfection using the DPc-incorporated micelles. The light irradiation (fluence: 5.4 J/cm^2) was performed after prolonged incubation (i.e. 24 h) with the pDNA- and DPc-incorporated micelles, followed by 48 h post-incubation in a fresh medium.

In conclusion, polymeric micelles might be a useful nanocarrier, which has been demonstrated to show prolonged blood circulation and thereby accumulate in the target tissues after intravenous administration, motivating us to study the PCI-mediated transfection using the combinational formulation of the pDNA- and DPc-incorporated micelles. Indeed, the PCI using the combinational micellar formulation achieved a remarkable photochemical enhancement of the transgene expression while maintaining an approximately 80% cell viability over a wide range of DPc concentrations and light doses. Thus, the usefulness of our strategy for *in vitro* trasnfection was successfully demonstrated. This system can be potentially useful for the gene therapy of solid tumors and ophthalmic diseases such as age-related macular regeneration (AMD) (Ideta et al. 2005). In addition to therapeutic genes, small interfering RNA (siRNA), which is known as the most powerful tool for sequence-specific silencing of the target genes (Elbashir et al. 2001), might also be delivered in a light-inducible manner by this strategy. The target-selective delivery of the therapeutic genes and siRNA

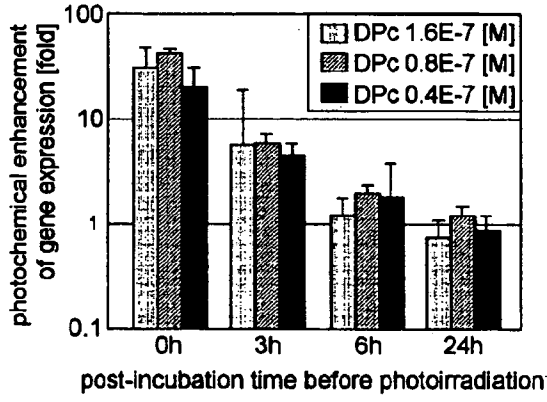

Figure 10. The effect of post-incubation time in the micelle-free medium before photoirradidation on the photochemical enhancement of the transfection of the polyplex micelles in the PCI-mediated transfection using the DPc-incorporated micelles. The cells were photoirradiated (5.4 J/cm^2) at defined post-incubation time after 6 h incubation with the pDNA- and DPc-incorporated micelles and medium replacement with a fresh one, followed by 48 h post-incubation.

by micellar nanocarriers followed by their light-induced activation at the target site might ensure the safety and effectiveness of *in vivo* gene and siRNA therapy. At present, this strategy could be applied only to the tissues, to which a visible light is accessible; however, recent advances in the laser technology such as a two-photon excitation laser (Oh et al. 1997) will solve the problems of limited tissue penetration of the light in the near future. We are now investigating *in vivo* PCI-mediated gene delivery using polymeric micelles via systemic administration and the results will be reported in a forthcoming paper.

Acknowledgements

The authors wish to express their gratefulness to the Health and Labor Sciences Research Grants in Research on Advanced Medical Technology in Nanomedicine Area from the Ministry of Health, Labor and Welfare (MHLW), Japan. Also, they wish to express their thanks for the Grant-in-Aid for Scientific Research, the Special Coordination Funds for Promoting Science and Technology and the Project on the Materials Development for Innovative Nano-Drug Delivery Systems from the Ministry of Education, Culture, Sports, Science and Technology (MEXT), Japan.

References

Bae Y, Nishiyama N, Fukushima S, Koyama H, Matsumura Y, Kataoka K. 2005. Preparation and biological characterization of polymeric micelle drug carriers with intracellular pH-triggered drug release property: Tumor permeability, controlled subcellular drug distribution, and enhanced *in vivo* antitumor efficacy. Bioconjug Chem 16:122–130.

Berg K, Selbo PK, Prasmikaite L, Tjelle TE, Sandvig K, Moan J, Gaudernack G, Fodstad O, Kjølsrud S, Anholt H, Rodal GH, Rodal SK, Høgset A. 1999. Photochemical internalization: A novel technology for delivery of macromolecules into cytosol. Cancer Res 59:1180–1183.

Elbashir SM, Harborth J, Lendeckel W, Yalcin A, Weber K, Tuschl T. 2001. Duplexes of 21-nucleotide RNAs mediate RNA interference in cultured mammalian cells. Nature 411:494–498.

Fukushima S, Miyata K, Nishiyama N, Kanayama N, Yamasaki Y, Kataoka K. 2005. PEGylated polyplex micelles from triblock cationers with spatially ordered layering of condensed pDNA and buffering units for enhanced intracellular gene delivery. J Am Chem Soc 127:2810–2811.

Harada A, Kataoka K. 1995. Formation of polyion complex micelles in an aqueous milieu from a pair of oppositely charged block copolymers with poly(ethylene glycol) segments. Macromolecules 28:5294–5299.

Harada-Shiba M, Yamauchi K, Harada A, Shimokado K, Kataoka K. 2002. Polyion complex micelles as a vector for gene therapy—pharmacokinetics and *in vivo* gene transfer-. Gene Ther 9:407–414.

Høgset A, Prasmickaite L, Tjelle TE, Berg K. 2000. Photochemical transfection: A new technology for light-induced, site-directed gene delivery. Hum Gene Ther 11:869–880.

Høgset A, Prasmickaite L, Hellum M, Engesæter BØ, Olsen VM, Tjelle TE, Wheeler CJ, Berg K. 2002. Photochemical transfection: A technology for efficient light-directed gene delivery. Somat Cell Mol Genet 27:97–113.

Høgset A, Prasmickaite L, Selbo PK, Hellum M, Engesæter BØ, Bondted A, Berg K. 2004. Photochemical internalization in drug and gene delivery. Adv Drug Deliv Rev 56:95–115.

Ideta R, Tasaka F, Jang W-D, Nishiyama N, Zhang G-D, Harada A, Yanagi Y, Tamaki Y, Aida T, Kataoka K. 2005. Nanotechnology-based photodynamic therapy for neovascular disease using a supramolecular nanocarrier loaded with a dendritic photosensitizer. Nano Lett 5:2426–2431.

Itaka K, Yamauchi K, Harada A, Nakamura K, Kawaguchi H, Kataoka K. 2003. Polyion complex micelles from plasmid DNA and poly(ethylene glycol)–poly(L-lysine) block copolymer as serum-tolerable polyplex system: Physicochemical properties of micelles relevant to gene transfection efficiency. Biomaterials 24:4495–4506.

Itaka K, Miyata K, Harada A, Kawaguchi H, Nakamura K, Kataoka K. 2004. Clinically available endosomolytic agent for gene delivery. In: Svenson S, editor. Carrier-based drug delivery. 879. Washington: ACS Symposium Series. p 154–159.

Jang W-D, Nishiyama N, Zhang G-D, Harada A, Jiang D-L, Kawauci S, Morimoto Y, Kikuchi M, Koyama H, Aida T, Kataoka K. 2005. Suparmolecular nanocarrier of anionic dendrimer porphyrins with PEGylated cationic block copolymer to enhance intracellular photodynamic efficacy. Angew Chem Int Ed 44:419–423.

Kataoka K, Kwon GS, Yokoyama M, Okano T, Sakurai Y. 1993. Block copolymer micelles as vehicles for drug delivery. J Control Release 24:119–132.

Kataoka K, Harada A, Nagasaki Y. 2001. Block copolymer micelles for drug delivery: Design, characterization and biological significance. Adv Drug Deliv Rev 47:113–131.

Katayose S, Kataoka K. 1997. Water-soluble polyion complex associates of DNA and poly(ethylene glycol)–p(L-lysine) block copolymer. Bioconjug Chem 8:702–707.

Kwon GS, Suwa S, Yokoyama M, Okano T, Sakurai Y, Kataoka K. 1994. Enhanced tumor accumulation and prolonged circulation times of micelle-forming poly(ethylene oxide-aspartate) block copolymer–Adriamycin conjugate. J Control Release 29:17–23.

Macdonald IJ, Dougherty TJ. 2001. Basic principle of photodynamic therapy. J Porphyrins Phthalocynanines 5: 105–129.

Merdan T, Kopecek J, Kissel T. 2002. Prospects for cationic polymers in gene and oligonucleotide therapy against cancer. Adv Drug Deliv Rev 54:715–758.

Miyata K, Kakizawa Y, Nishiyama N, Harada A, Yamasaki Y, Koyama H, Kataoka K. 2004. Block catiomer polyplexes with regulated densities of charge and disulfide cross-linking directed to enhance gene expression. J Am Chem Soc 126: 2355–2361.

Moan J, Berg K, Anholt A, Madslien K. 1994. Sulfonated aluminum phthalocyanines as sensitizers for photochemotherapy. Effects of small doses on localization, dye fluorescence and photosensitivity in V79 cells. Int J Cancer 58:865–870.

Ng ACH, Li X, Ng DKP. 1999. Synthesis and photophysical properties of nonaggregated phthalocyanines bearing dendritic substitutes. Macromolecules 32:5292–5298.

Nishiyama N, Stapert HR, Nagano T, Takasu D, Jiang D-L, Aida T, Kataoka K. 2003a. Light-harvesting ionic dendrimer porphyrins as new photosensitizers for photodynamic therapy. Bioconjug Chem 14:58–66.

Nishiyama N, Okazaki S, Cabral H, Miyamoto M, Kato Y, Sugiyama Y, Nishio K, Matsumura Y, Kataoka K. 2003b. Novel cisplatin-incorporated polymeric micelles can eradicate solid tumors in mice. Cancer Res 63:8977–8983.

Nishiyama N, Iriyama A, Jang W-D, Miyata K, Itaka K, Inoue Y, Takahashi H, Yanagi Y, Tamaki Y, Koyama H, Kataoka K. 2005. Light-induced gene transfer from packaged DNA enveloped in a dendrimeric photosensitizer. Nat Mater 4:934–941.

Nishiyama N, Kataoka K. 2006. Nano-structured devices based on block copolymer assemblies for drug delivery: designing structures for enhanced drug function. Adv Polym Sci 193:67–101.

Niwa H, Yamamura K, Miyazaki J. 1991. Efficient selection for high-expression transfectants with a novel eukaryotic vector. Gene 108:193–199.

Ogris M, Wagner E. 2002. Targeting tumors with non-viral gene delivery systems. Drug Discov Today 7:479–485.

Oh DH, Stanley RJ, Lin M, Hoeffler WK, Boxer SG, Berns MW, Bauer E. 1997. Two-photon excitation of 4′-hydroxymethyl-4,5′,8-trimethylpsoralen. Photochem Photobiol 65:91–95.

Pack DW, Hoffman A, Pun S, Stayton PS. 2005. Design and development of polymers for gene delivery. Nat Rev Drug Discov 4:581–593.

Prasmickaite L, Høgset A, Berg K. 2001. Evaluation of different photosensitizers for use in photochemical gene transfection. Photochem Photobiol 73:388–395.

Stapert HR, Nishiyama N, Jiang D-L, Aida T, Kataoka K. 2000. Polyion complex micelles encapsulating light-harvesting ionic dendrimer zinc porphyrins. Langmuir 16:8182–8188.

Takakura Y, Hashida M. 1996. Macromolecular carrier systems for targeted drug delivery: Pharmacokinetic considerations on biodistribution. Pharm Res 13:820–831.

Wakebayashi D, Nishiyama N, Yamasaki Y, Itaka K, Kanayama N, Harada A, Nagasaki Y, Kataoka K. 2004. Lactose-conjugated polyion complex micelles incorporating plasmid DNA as a targetable gene vector system: Their preparation and gene transfecting efficiency against cultured HepG2 cells. J Control Release 95:653–664.

Development of a Fitting Model Suitable for the Isothermal Titration Calorimetric Curve of DNA with Cationic Ligands

Wankee Kim,[†] Yuichi Yamasaki,*[,†] and Kazunori Kataoka*[,†,‡]

Department of Materials Science and Engineering, School of Engineering, The University of Tokyo, 7-3-1 Hongo, Bunkyo-ku, Tokyo 113-8656, Japan, and Center for Disease Biology and Integrative Medicine, Graduate School of Medicine, The University of Tokyo, 7-3-1 Hongo, Bunkyo-ku, Tokyo 113-0033, Japan

Received: December 28, 2005; In Final Form: April 12, 2006

A novel curve fitting model was developed for the isothermal titration calorimetry (ITC) of a cationic ligand binding to DNA. The ligand binding often generates a DNA conformational change from an elongated random coil into a compact collapsed form that is referred to as "DNA condensation". The ligand binding can be classified into two regimes having different binding constants K_i, i.e., the binding to an elongated DNA chain with a binding constant K_1 and with K_2 that occurred during the conformational transition. The two-variable curve fitting models are usually bound by a strict regulation on the difference in the values of the binding constants $K_1 > K_2$. For the DNA condensation, however, the relationships for K_1 and K_2 are still unclear. The novel curve fitting model developed in this study takes into account this uncertainty on the relationship of the binding constants and is highly flexible for the two-variable binding constant system.

Introduction

Isothermal titration calorimetry (ITC) is a useful method to explore the interaction between DNA and cationic ligands.[1−10] By adding a solution of cationic ligands to a DNA solution, the ITC instrument measures the heat accompanied by the binding reaction. The thermodynamic parameters such as changes in enthalpy, entropy, and free energy can be obtained by fitting the ITC curve to an adequate curve fitting model. Nevertheless, general curve fitting models are useful only for simple binding systems, and they may not be applied to particular cases such as DNA condensation.

In general, there are three kinds of curve fitting models, i.e., the single set of identical sites (SSIS) model, two sets of independent sites (TSIS) model, and sequential binding sites (SBS) model.[11,12] The SSIS model satisfies many ligand binding systems when all the binding sites on the substance are identical. The following parameters, stoichiometry N, binding constant K, and change in enthalpy ΔH can be obtained using this fitting model. The TSIS model, which is useful when substances have two kinds of binding sites, enables us to calculate both sets of parameters N_1, K_1, ΔH_1 and N_2, K_2, ΔH_2 for the first and second ligand bindings. While the TSIS model seems to be well adapted to various cases, it should not be applied to the particular system where K_1 is smaller than K_2, because this model is constructed assuming that K_1 is larger than K_2. The SBS model is appropriate for the system, such as the binding of multiple ligands to transition metal ions, for example, the binding of four Br^- ions to Cd^{2+} leading to $CdBr_4^{2-}$. For this case, the number of sequential sites should be integral. The absence of a parameter equivalent to N indicates that the curve fitting is carried out by changing only two parameters, K and H, on each site.

Concerning the binding of cationic ligands to DNA, a conformational change in the DNA chain may affect their binding behavior. The DNA chain collapses after some fraction of negative charges on the phosphate backbone is neutralized by cationic ligands, which is referred to as DNA condensation. The binding process of cationic ligands to DNA can be classified into two parts, a simple binding without a DNA conformational transition and another binding event that followed during the conformational transition. The binding constant for the former is K_1 and that for the latter is K_2. During the beginning of ligand binding, the former binding process proceeds where the DNA chains retain their conformation. Consequently, the latter binding occurs after the former was completed, resulting from the DNA conformational transition.

This scheme is consistent with the prediction of the counterion condensation (CC) theory developed by Oosawa and Manning and with the experimental results obtained from electrophoresis.[13] The CC theory indicates the presence of critical residual charges on elongated DNA chains that results from the former ligand binding. While the degree of charge neutralization depends on the ligand concentration, the critical value of charge neutralization is determined by their valence. For example, the values of DNA in the presence of monovalent, divalent, and trivalent cations are 0.76, 0.88, and 0.92, respectively.[14] Bloomfield concluded that the DNA chains retain their conformation until the degree of charge neutralization is increased to 0.90, indicating that cationic ligands with their valence equal to or grater than 3 possesses the potential to generate DNA condensation. On the contrary, it was clarified that almost all of the negative charges are neutralized in the collapsed state.[15] These experimental results suggest that the DNA conformation and its residual charges correlate with each other, and that the binding manner of the cationic ligands is also affected by DNA conformation. Therefore, the binding classification described above is appropriate for the ligand binding to DNA phosphates.

* To whom correspondence should be addressed: Kazunori Kataoka, tel +81-3-5841-7138, fax +81-3-5841-7139, e-mail kataoka@bmw.t.u-tokyo.ac.jp; Yuichi Yamasaki, tel +81-3-5841-7145, fax +81-3-5841-7139, e-mail yamasaki@bmw.t.u-tokyo.ac.jp.

† Department of Materials Science and Engineering, School of Engineering, The University of Tokyo.

‡ Center for Disease Biology and Integrative Medicine, Graduate School of Medicine, The University of Tokyo.

10.1021/jp057554e CCC: $33.50
Published on Web 05/17/2006

To obtain thermodynamic parameters from the ITC measurements, the suitable fitting model should be carefully chosen by considering the relationship of the magnitude of the binding constants. For the DNA condensation, however, this relationship has so far been unknown. Recently, Teif and Lando theoretically pointed out that the DNA conformational change to the collapsed state takes place when $K_2 > K_1$.[16] Actually, Mel'nikov et al. reported the cooperative binding observed in the transition region of the DNA condensation induced by a cationic surfactant.[17] Thus, we developed a novel fitting model suitable for this situation $K_2 > K_1$ to analyze the binding isotherm obtained from the DNA condensation. In this paper, the binding isotherms obtained from the DNA condensation induced by a low molecular weight condensing reagent, cobalt hexamine ($Co(NH_3)_6^{3+}$), and by a polymeric cation poly(ethylene glycol)–poly(L-lysine) block copolymer (PEG–PLL), are demonstrated as typical examples. The former is treated as a standard chemical of a DNA condensation investigation[18] and the latter as a promising polycation as a gene carrier.[19] A comparison of both binding isotherms and the validity of the novel fitting model will be discussed in detail.

Experimental Section

Materials. The plasmid pGL3 DNA (5256 base pairs) was purchased from Promega (Madison, WI). The plasmid DNA (pDNA) was amplified in competent DH5α *Escherichia coli* and purified using the Qiafilter giga kit (QIAGEN, Germany). A stock solution of pDNA was prepared by dissolving purified pDNA in Millipore grade water containing 10 mM NaCl without any buffer solution. The DNA concentration was determined by the absorption at 260 nm. The PEG–PLL block copolymer with the average PEG molecular weight of 12 000 and the average degree of lysine polymerization of 109 was used in this study. The PEG–PLL block copolymer was prepared as already prescribed.[20] Let us now briefly explain the synthesis. PEG–PLL was synthesized using α-methoxy-ω-amino-PEG to initiate polymerization of the *N*-carboxy anhydride of the *Z*-protected lysine. The length of the lysine segment was regulated by the ratio of the monomer to PEG initiator. The deprotection of lysine was carried out under acidic conditions. ^{1}H NMR and size exclusion chromatography were employed for characterization of this block copolymer. The degree of polymerization is deduced by the ratio of the methylene proton of PEG to that on the lysine residue. Cobalt(III) hexamine trichloride was obtained from Wako Pure Chemicals (Osaka, Japan) and used as received.

Isothermal Titration Calorimetry. Isothermal titration calorimetry (ITC) was performed using a Microcal VP-ITC calorimeter (Northampton, MA) with the normal cell (1.4643 mL) at 30 °C. Two milliliters of pDNA solution (0.3 mM in phosphate) was poured inside the cell after three rinses with 10 mM NaCl solution. The condensing agents were titrated into the pDNA solutions using an injection syringe. The concentrations of cobalt hexamine and PEG–PLL were chosen to be 1.2 and 3 mM (in lysine unit), respectively. Each titration consisted of a preliminary 1-μL injection followed by 29 subsequent 10-μL injections at 3-min intervals. Control experiments were carried out for both ligands to determine the heats of ligand dilution, because the dilution effect should be subtracted to obtain the heat of binding. Prior to the ligand binding experiments, the calorimeter was verified by carrying out the Tris base protonation reaction with hydrochloric acid ($\Delta H = -13.58$ kcal/mol).

Analysis of ITC Curve. The analysis of the obtained ITC curves was performed using origin software with version 5.0 attached to the instrument. First, the integrated ITC curves were obtained from the raw data of the power change at each injection, using the add-on module for the purpose in the software, and then the fittings of those data to the fitting function developed here were performed to obtain the thermodynamic parameters, using a fitting tool prepared in the software, which was based on the Levenberg–Marquardt nonlinear fitting algorithm.

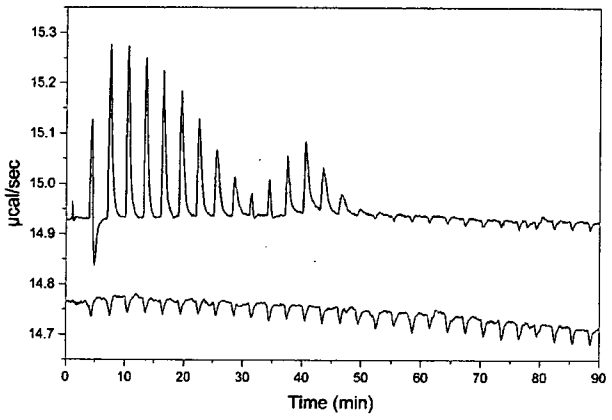

Figure 1. Raw data of ITC measurement for cobalt hexamine binding to plasmid pGL3 DNA in 10 mM NaCl aqueous solution. The upper curve shows the heats resulting from the titration of cobalt hexamine to pDNA solution. The lower curve was obtained by the titration without pDNA, indicating the heats generated by the dilution of the ligand solution. To obtain the ITC binding curves, the lower one should be subtracted from the upper one.

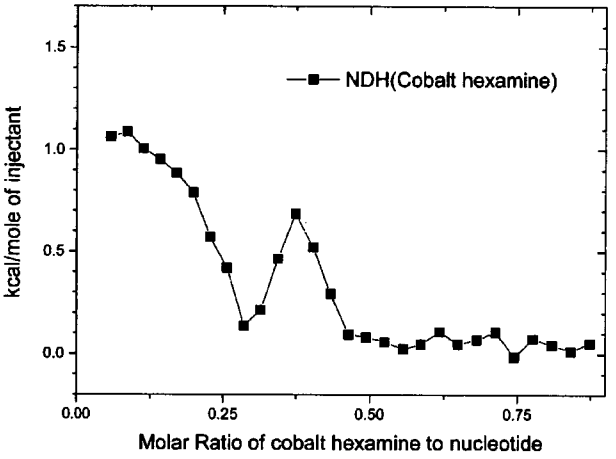

Figure 2. Integrated ITC curve of cobalt hexamine binding to plasmid pGL3 DNA in 10 mM NaCl aqueous solution. This ITC binding curve was calculated from both curves in Figure 1. Endothermic two-stage binding was observed during this ligand binding.

Results

Typical nonintegrated titration curves are shown in Figure 1. The upper curve was obtained by titrating pDNA with cobalt hexamine, and the lower curve was obtained without pDNA indicating the heat of the dilution of cobalt hexamine solution. The upper curve includes the heats resulting from both the dilution effect and the binding reaction. To obtain integrated binding curves as shown in Figure 2, the peaks of both curves were integrated and the latter was subtracted from the former. Figure 2 indicates that the binding of cobalt hexamine onto pDNA can be classified into two stages. Endothermic events were observed during both stages, suggesting that this binding

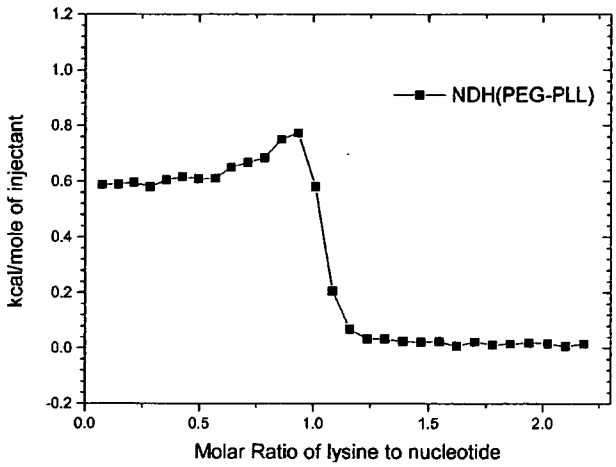

Figure 3. Integrated ITC curve of PEG–PLL binding to plasmid pGL3 DNA in water with 10 mM NaCl. The endothermic binding was completed by the charge ratio of 1.2.

was entropically driven. This result is in good agreement with those reported by other researchers.[2,4]

In this system, the initial binding stage was completed with the charge ratio of 0.9. The second stage was observed when a further addition of cobalt hexamine occurred. No heat was generated at the region in the charge ratio range higher than 1.5. From the results of turbidity measurement, a significant decrease in the transmittance resulting from the formation of aggregates was observed immediately following the second binding stage (data not shown). After the titration measurement, precipitates were visually observed in the sample solution.

The integrated ITC curve of the PEG–PLL binding to pDNA is shown in Figure 3, indicating an endothermic ligand binding the same as that observed in the $Co(NH_3)_6^{3+}$/pDNA system. Although the two-stage binding observed in the ITC curve of the cobalt hexamine titration is well separated, no segregation was observed in the ITC profile for the PEG–PLL/pDNA system. The PEG–PLL binding was completed with the charge ratio of 1.2.

Development of the Novel Fitting Model

A novel fitting model is based on the combination of the single set of identical sites (SSIS) model. Let us introduce the SSIS model as follows.[11,12] Generally, the binding constant K and the relationship of the total and free ligand concentrations (X_t and $[X]$) are represented by eqs 1 and 2, respectively

$$K = \frac{\Theta}{(1-\Theta)[X]} \quad (1)$$

$$X_t = [X] + N\Theta M_t \quad (2)$$

where N is the number of binding sites, M_t is the total concentration of macromolecule, and Θ is the fractional sites occupied by ligand. Combining eqs 1 and 2 gives eq 3

$$\Theta^2 - \Theta\left[1 + \frac{X_t}{NM_t} + \frac{1}{NKM_t}\right] + \frac{X_t}{NM_t} = 0 \quad (3)$$

The total heat content Q of the solution contained in the sample cell at fractional saturation Θ is

$$Q = N\Theta M_t \Delta H V_0 \quad (4)$$

where ΔH is the molar heat of ligand binding and V_0 is the cell

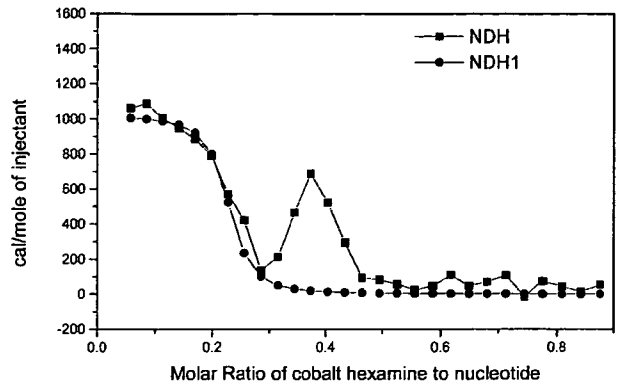

Figure 4. Integrated ITC curve of cobalt hexamine binding to plasmid pGL3 DNA (■) and representative ITC curve NDH1 generated from the SSIS model with the following fitting parameter (●). $N_1 = 0.216 \pm 0.004$, $K_1 = (17.79 \pm 4.99) \times 10^5\ M^{-1}$, $\Delta H_1 = 1019 \pm 30$ cal/mol.

volume. Solving the quadratic eq 3 for Θ and then substituting this into eq 4 gives eq 5

$$Q = \frac{NM_t\Delta HV_0}{2}[1 + (X_t/NM_t) + (1/NKM_t) - \sqrt{(1 + (X_t/NM_t) + (1/NKM_t))^2 - (4X_t/NM_t)}] \quad (5)$$

The value of Q can be calculated for any designated values of N, K, and ΔH at the end of the ith injection and designated $Q(i)$. The parameter of interest for comparison with the experiment, however, is the change in heat content from the completion of the $(i-1)$th injection to completion of the i-th injection. The expression for Q in eq 5 only applies to the liquid contained in volume V_0. Therefore, after an injection is completed, it is obvious that a correction must be made for the displaced volume (i.e., ΔV_i = injection volume) since some of the liquid in V_0 after the $(i-1)$th injection will no longer be in V_0 after the ith injection, even though it will contribute to the heat effect (assuming that the kinetics of the reaction and mixing are fast) before it passes out of the working volume V_0. The liquid in the displaced volume contributes about 50% as much heat effect as an equivalent volume remaining in V_0. The correct expression for the heat released $\Delta Q(i)$ from the ith injection is

$$\Delta Q(i) = Q(i) + \frac{dV_i}{V_0}\left[\frac{Q(i) + Q(i-1)}{2}\right] - Q(i-1) \quad (6)$$

By dividing $\Delta Q(i)$ with moles in the ith injected volume, the normalized heat, NDH(i), is obtained. Hereafter, NDH(i) is described by NDH(N, ΔH, K) because NDH(i) is dependent on the three parameters, N, ΔH and K.

A set of fitting parameters, N_1, K_1, and ΔH_1, is assigned to the initial binding stage of cationic ligands to the elongated pDNA, and another set, N_2, K_2, and ΔH_2, is assigned to the second binding stage during the pDNA conformational transition. On the basis of the SSIS model, the optimum fitting parameters for the initial stage provide the most suitable ITC curve as shown in Figure 4.

On comparison of the ITC curves for the PEG–PLL/pDNA system with that for $Co(NH_3)_6^{3+}$/pDNA, the molar ratios where the second binding stage appeared disagree. It is assumed that the second binding stage in the PEG–PLL system is immediately generated after the initial binding stage. In the system of cobalt hexamine, however, the generation of the second stage requires an excess amount of ligand in the bulk solution, corresponding to the delay of the second stage in Figure 2. As

shown in Figure 3, the second stage in the PEG−PLL system was almost finished around the charge equivalent condition. Therefore, both the initial and second binding stages in the PEG−PLL system coexist in a certain region where the molar ratio is greater than 0.5. This binding feature agrees with the results obtained from the direct observation of the DNA condensation using fluorescence microscopy.[21]

On the contrary, the two binding stages were well separated in the system of cobalt hexamine. In this system, the second binding stage during the DNA conformational change occurs after the initial stage where the fraction of the bound ligand reaches the critical one and all of the injected cationic ligands are consumed in the initial binding stage. As the injections of the cationic ligands are repeated, the amount of bound ligands gradually increases and reaches a maximum value at the molar ratio of 0.3, corresponding to the critical residual charges of the elongated DNA double helices, i.e., the end point of the initial binding stage. Under this condition, the added ligands do not tend to bind the elongated DNA, then the heat generated by the binding gradually decreases. The further addition of cationic ligands induces the DNA conformational change or "DNA condensation". During this transition, the second binding stage of the cationic ligands is promoted. The presence or absence of the delay between the two binding stages seems to be a significant phenomenological difference. Therefore, the effect of this delay is taken into consideration in the novel fitting model developed in this study.

Prior to describing the delay of the second binding stage observed in the $Co(NH_3)_6^{3+}$/pDNA system, the curve fitting for the second binding stage should be discussed here. On the basis of the SSIS model, a general ITC curve should be produced as a decreased sigmoidal curve as shown in Figure 4 (NDH1). According to the results of the DNA conformational analysis under fluorescence microscopy, both the elongated and collapsed DNA chains coexist during the transition region of the DNA condensation.[22] Thus, the population of collapsed DNAs should gradually increase with an increase in the molar ratio. This leads to the decrease in the fraction of ligands bound to the elongated DNA and the increase in that of the collapsed one. If the delay in the second binding stage was missing, the residual ligands not involved in the initial binding stage ideally contribute to the second binding stage. The amount of this residual ligand is represented by differences between the maximum and each fraction of the binding ligand, which can be expressed by an increased sigmoidal curve. Because the sigmoidal NDH having N, K, ΔH as a variable is linearly dependent on the fraction of ligands (Θ), Θ can be described as the absolute value of NDH divided by ΔH, ABS(NDH/ΔH).

To describe the fraction of the occupied site on DNA during the second binding stage, an NDH3 sigmoidal curve was employed. The definition of parameters for NDH3 is basically the same as those for the NDH1, but only N_3 is variable when considering the delay of the second binding stage. When N_3 is equal to N_1, the initial binding stage is immediately followed by the second binding stage during the DNA condensation. On the contrary, as N_3 becomes larger than N_1, the second binding stage is separated from the initial binding stage, indicating that the delay in the second stage is significant in the ITC curve. Thus, the fraction of the occupied site on DNA during the second stage is represented by ABS((ΔH_1 − NDH3)/ΔH_1) in Figure 5, which is derived from 1 − ABS(NDH3/ΔH_1). We intend to generate for the second binding stage the NDH2 curve which is a function of N_2, K_2, and ΔH_2. The second binding stage of the ITC curve was fitted by the product of the

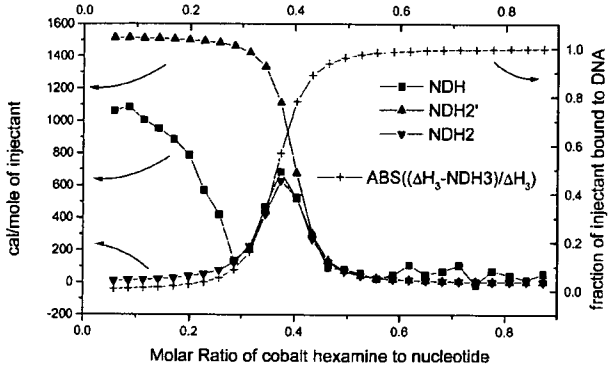

Figure 5. Representative curve for the second binding stage during pDNA condensation (NDH2; ▼).

hypothetical ITC curve NDH2′ and the increased sigmoidal curve ABS((ΔH_1 − NDH3)/ΔH_1). The ITC curve NDH2′ that corresponds to a standard ITC curve with the absence of the initial binding stage is generated by the SSIS model, indicating that the NDH2′ curve is defined by N_2', K_2', and $\Delta H_2'$. The product was defined as NDH2 where N_2' − N_3 (the difference of N_2' and N_3), K_2', and $\Delta H_2'$ are selected for N_2, K_2, and ΔH_2, respectively.

Application of New Model

The optimum fittings for the experimental ITC curves of both $Co(NH_3)_6^{3+}$/pDNA and PEG−PLL/pDNA are shown in Figures 6 and 7, respectively. The ITC curves were fitted by the sum of NDH1 and NDH2, corresponding to the initial and second binding stages, respectively. The sum of these two curves represents the relation of the total heats accompanied by ligand binding on DNA to the mixing ratio. Although the curve NDH1 is defined by the set of three parameters, N_1, K_1, and ΔH_1, another curve, NDH2, was defined by the set of six parameters, N_3, K_1, ΔH_1, N_2', K_2', and $\Delta H_2'$. In this method, both curves, NDH1 and NDH2, were simultaneously fitted. The difference in N_2' and N_3, which is described by N_2, means the binding stoichiometry for the second binding stage in the novel fitting model, and the difference in N_1 and N_3 reflects the delay of the second binding stage. The important thermodynamic parameters are listed in Tables 1 and 2. For both the simplified notation and comparison with the reported data, the binding stoichiometry for the second binding stage is represented by the parameter N_2 in the tables.

Discussion

The cooperative binding of polycations to DNA chains has been discussed as a typical binding feature of polyelectrolytes. Similar binding processes have already been independently considered by McGhee and von Hippel[23] and by Schwarz.[24] MaGhee and von Hippel suggested the concept of cooperativity of protein binding to DNA using the following three binding modes: (1) the binding to the isolated site with an intrinsic binding constant K, (2) a singly contiguous site to which a linear polymer binds with binding constant $K\omega$, and (3) a doubly contiguous site to which a linear polymer binds with binding constant $K\omega^2$, where ω is the cooperativity constant. When $\omega > 1$, the cationic ligands attract each other and the binding is positively cooperative; when $\omega < 1$, the cationic ligands repel each other and the binding is anti or negatively cooperative; when $\omega = 1$, neither cooperativity is observed during the binding.

Schwarz's theory also implies two types of intrinsic binding processes: (1) the binding of isolated ligands with binding

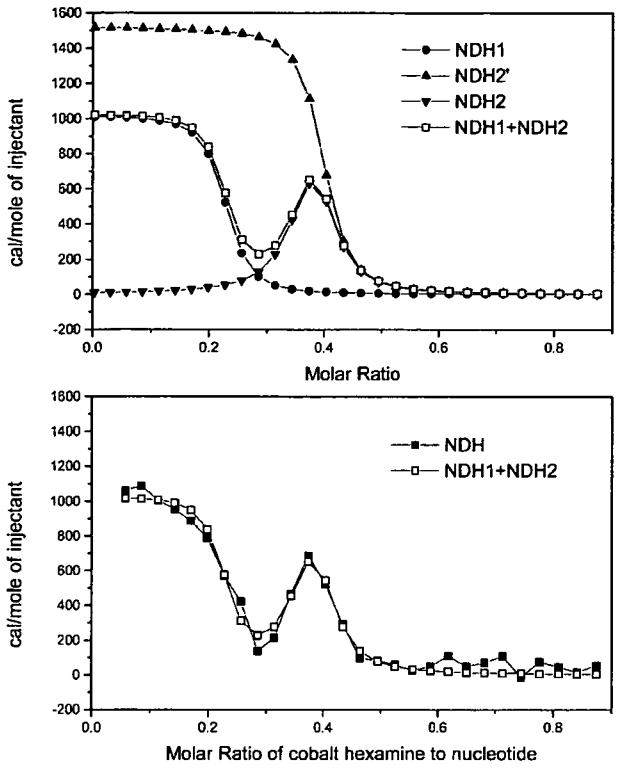

Figure 6. Optimum fitting for the experimental ITC curve (■) of $Co(NH_3)_6^{3+}$/pDNA, NDH1 + NDH2 (□). NDH1 (●) represents the initial binding stage corresponding to that in Figure 4. NDH2′ (▲) and NDH2 (▼) are the same as those in Figure 5. NDH1 + NDH2 is used for the fitting of the experimental ITC curve; $N_1 = 0.216 \pm 0.004$, $K_1 = (17.79 \pm 4.99) \times 10^5\ M^{-1}$, $\Delta H_1 = 1019 \pm 30$ cal/mol, $N_2' = 0.385 \pm 0.012$, $N_3 = 0.354$, $N_2 = N_2' - N_3 = 0.031 \pm 0.012$, $K_2 = K_2' = (27.82 \pm 12.61) \times 10^5\ M^{-1}$, $\Delta H_2 = \Delta H_2' = 1520 \pm 301$ cal/mol.

constant K (nucleation), and (2) the binding of ligands to the nearest-neighbor binding site (aggregation) with binding constant Kq, where q is the cooperativity parameter. In both models, the binding process with the binding constant $K\omega$ or Kq is generated by the initial ligand binding with binding constant K, which is the matter of our concern. Let us assume that K_2 was equal to $K\omega$ or Kq. For the cobalt hexamine binding to DNA, ω or q is estimated to be 1.56, which is obtained by K_2/K_1 using the parameters shown in Table 1. For the PEG−PLL binding to DNA, ω or q is estimated to be 19.20 using the parameters shown in Table 2. In both cases, it is obvious that the binding constant K_2 seems to be significantly enhanced and the estimation for the cobalt hexamine binding is inconsistent with the reported data.[2] Although the above classification was suggested to explain the cooperative binding of the cationic ligands, it is not clear in this study whether such kinds of cooperativities induced by the ligand−ligand interactions exist in the binding of the cobalt hexamine or PEG−PLL to pDNA.

In this study, it was assumed that the positive cooperative binding of the cobalt hexamine or PEG−PLL to DNA is attributed to the conformational change in DNA rather than the interaction between the same chemicals. The DNA conformational change produces the environmental modulation around the DNA vicinity, and this may affect the binding features of the cationic ligands. Hud et al. suggested that the effect of the DNA segment fluctuation induces the enhanced binding of cationic ligands to a loop formed by two sequence-separated sections in close contact.[25] The cationic ligands bind to this contact and stabilize the loop. Successive ligands bind both the

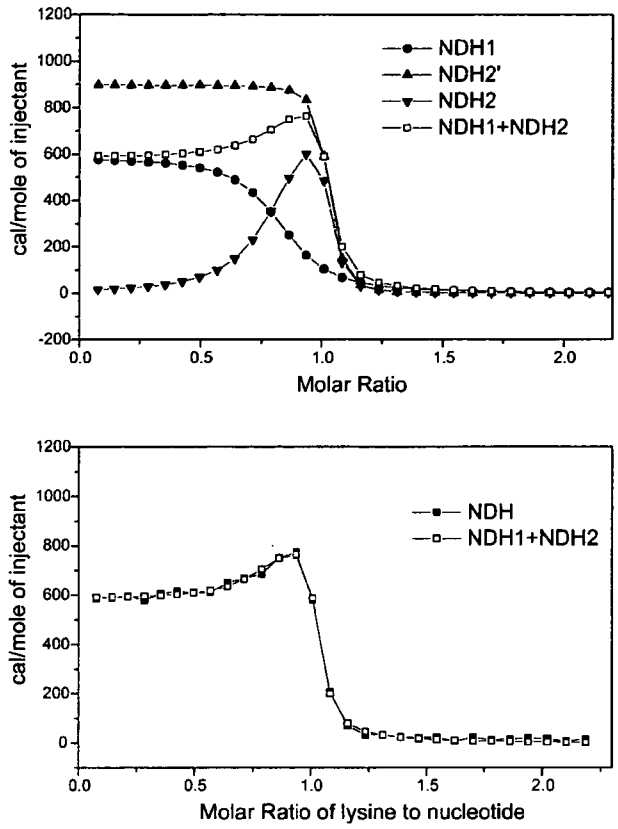

Figure 7. Optimum fitting for the experimental ITC curve (■) of PEG−PLL/pDNA, NDH1 + NDH2 (□). NDH1 (●) represents the initial binding stage corresponding to those of the PEG−PLL/pDNA system shown in Figures 5 and 6. NDH2′ (▲) and NDH2 (▼) correspond to those in Figure 6. NDH1 + NDH2 is used for the fitting of the experimental ITC curve: $N_3 = N_1 = 0.810 \pm 0.026$, $K_1 = (2.66 \pm 0.62) \times 10^5\ M^{-1}$, $\Delta H_1 = 585 \pm 5$ cal/mol, $N_2' = 0.994 \pm 0.005$, $N_2 = N_2' - N_3 = 0.184 \pm 0.031$, $K_2 = K_2' = (51.07 \pm 13.98) \times 10^5\ M^{-1}$, $\Delta H_2 = \Delta H_2' = 899 \pm 37$ cal/mol.

loop and extended DNA to induce the collapsed form. Therefore, the binding constants K_1 and K_2 are treated as individual variables in this study.

To develop a flexible fitting method, different types of ligands, a low-molecular weight metal complex cobalt hexamine and block copolymer PEG−PLL, were employed in this study. Cobalt hexamine is a widely used chemical as a standard reagent of DNA condensation. On the contrary, PEG−PLL is a relatively recently developed reagent as a gene carrier.[19] As exemplified by the presence or absence of the delay in the appearance of the second binding stage in Figures 2 and 3, the condensation mechanism seems to be slightly different from each other despite the same driving force, the electrostatic interaction. It was reported that this difference becomes enhanced in the dilute DNA solution experiments and the latter more effectively induces the DNA condensation.[21]

Under such situations, the charge equivalent mixing ratio between PEG−PLL and DNA is enough to induce the DNA condensation, while an excess amount of cobalt hexamine, at least several times that of the phosphate residue, should be required. A similar trend was observed in the ITC curves obtained in this study. The charge ratio at the end point of the PEG−PLL titration was 1.2, while that of cobalt hexamine was slightly higher than this value. This difference was mainly caused by their chemical structures. In this study, a simple comparison of the thermodynamic parameters N_1 and K_1 in the

TABLE 1: Parameters Obtained by Various Fitting Methods

	N_1	$K_1/10^5$ (M^{-1})	ΔH_1 (cal/mol)	N_2	$K_2/10^5$ (M^{-1})	ΔH_2 (cal/mol)
this work[a]	0.216 ± 0.004	17.79 ± 4.99	1019 ± 30	0.031 ± 0.012	27.82 ± 12.61	1520 ± 301
ref 2[b]	0.217 ± 0.012	2.30 ± 0.80	1240 ± 100	0.059 ± 0.012	6.00 ± 1.60	820 ± 90
origin[c]	0.218 ± 0.010	74.02 ± 142.4	1086 ± 68	not converged		

[a] This work: developed by this work. [b] ref 2: reported in reference 2. [c] Origin: by applying the two sets of independent sites (TSIS) model to each binding process divided from the experimental ITC curve shown in Figure 2, which is the same method as that used in the ref 2. $N_2' = 0.385 \pm 0.012$, $N_3 = 0.354$, $N_2 (=N_2' - N_3) = 0.031 \pm 0.012$, $K_2 = K_2'$, $\Delta H_2 = \Delta H_2'$.

TABLE 2: Parameters Obtained by Various Fitting Methods

	N_1	$K_1/10^5$ (M^{-1})	ΔH_1 (cal/mol)	N_2	$K_2/10^5$ (M^{-1})	ΔH_2 (cal/mol)
this work[a]	0.810 ± 0.026	2.66 ± 0.62	585 ± 5	0.184 ± 0.031	51.07 ± 13.98	899 ± 37
origin[b]	0.781 ± 0.032	139.10 ± 44.19	584 ± 9	0.222 ± 0.034	7.2 ± 2.23	973 ± 77

[a] This work: developed by this work. [b] Origin: by applying TSIS model to the ITC curve shown in Figure 3. $N_3 = N_1$, $N_2' = 0.994 \pm 0.005$, $N_2 (=N_2' - N_3) = 0.184 + 0.031$, $K_2 = K_2'$, $\Delta H_2 = \Delta H_2'$.

cobalt hexamine system with those of PEG−PLL makes no realistic sense, because the former was analyzed in a molar unit and the latter was summarized in a charge unit. On comparison of N_1 with the consideration of the valency, however, it is obvious that PEG−PLL more effectively binds (see Tables 1 and 2).

In the novel fitting model developed in this study, the cationic ligand binding to DNA was classified into two stages, the initial and second binding stages. The former has the binding constant K_1 and the latter K_2. Regarding the magnitude relationship of the binding constants, Teif and Lando theoretically pointed out that the DNA conformational change to the collapsed state takes place when $K_2 > K_1$.[16] In the general curve fitting models for the experimental ITC curves, however, this assumption could not be taken into consideration. Although general fitting models that can treat multiple binding sites have the assumption $K_1 > K_2$, our model is not restricted by this assumption. To treat two binding stages as individual events, they were characterized in relation to the conformational change in pDNA. Thus, the former occurs when the DNA conformation retained as the elongated state and the latter is promoted during the DNA conformational change.

Generally, there is a significant difficulty in the separation of the two binding stages, when the overlap of the initial and second binding stages was observed as shown in the PEG−PLL system. Despite the absence of the saddle point in the integrated ITC curve for the PEG−PLL system, the assumption of two-stage binding is plausible, because the discrete transition between the elongated and collapsed states was essentially the same as that observed in the cobalt hexamine system.[21] Table 1 shows a comparison of the thermodynamic parameters determined in this study with those by other methods reported in ref 2 and obtained by the manufacturer recommended method that is based on the two sets of independent sites (TSIS) model. Although the second set of parameters did not converge using the TSIS model, no significant difference was observed in both values of N_1 and N_2. As mentioned in the Introduction, the TSIS model should not be applied to the particular system where K_1 is smaller than K_2, because this model is constructed assuming that K_1 is greater than K_2. This is the reason the second set of parameters was not determined by the TSIS model.

Matulis et al. also employed the TSIS model, but they completely divided the integrated ITC curve by the saddle point. In their method, two parts of the ITC curve were separately fitted.[2] Therefore, the magnitude relationship of K_1 and K_2 would not be discussed under their framework. On the contrary, both parts were simultaneously fitted in this study. In addition, when their method was applied to the PEG−PLL system, the curve fitting was done under the restricted assumption $K_1 > K_2$. However, our method is not restricted by this assumption. Among these three methods, thus, an appropriate method suitable for the discussion on the magnitude relationship of K_1 and K_2 is considered to be limited to the novel method developed in this study.

The charge ratio of the cationic ligands to DNA is expressed by the total stoichiometry, the sum of N_1 and N_2. On the basis of the consideration of the valence of cobalt hexamine, the charge ratio is estimated to be 0.72 in this study, suggesting that the residual ligands do not directly contribute to the DNA condensation (see Table 1). This trend is consistent with another report.[2] It is still controversial that the results of the ITC experiments disagree with the theoretical prediction of the two-variable counterion condensation theory.[14] As for the PEG−PLL system, the charge ratio was determined to be 0.99, indicating that almost all of the negative charge of the DNA phosphate is neutralized by the ligand binding (see Table 2). The result of the charge equivalent complexation agrees with those obtained from the single molecule observation under fluorescence microscopy.[20] This difference in the binding stoichiometry between cobalt hexamine and PEG−PLL reflects the strength of the electrostatic interaction between the cationic ligands and DNA phosphates.

Conclusion

The novel fitting method based on the SSIS model for the experimental ITC curve was developed and applied to the cationic ligands binding to DNA, cobalt hexamine, and PEG−PLL systems in this study. It is demonstrated that this curve fitting method can be applicable for both systems. As for the cobalt hexamine system, the thermodynamic parameters obtained by the novel fitting method have a similar trend with those reported by other researchers. It was suggested that this method is applicable for the PEG−PLL system, in which the separation of the two binding events is not enough for the appearance of the experimental ITC curve. Although other fitting methods are applicable under the restricted assumption $K_1 > K_2$, our method, unrestricted by this assumption, is widely applicable for both cases, $K_1 > K_2$ and $K_2 > K_1$.

Acknowledgment. We thank Mr. S. Fukushima of Nippon Kayaku Co., Ltd., Japan, for the kind donation of the PEG−PLL block copolymer. This work was partially supported by a grant-in-aid for scientific research from the Ministry of Education, Culture, Sports, Science, and Technology of Japan (MEXT), the Core Research Program for Evolutional Science and Technology (CREST) from the Japan Science and Technol-

ogy Agency (JST), and 21st century COE program "Human-Friendly Materials based on Chemistry" from MEXT.

References and Notes

(1) Spink, C. H.; Chaires, J. B. *J. Am. Chem. Soc.* **1997**, *119*, 10920−10928.

(2) Matulis, D.; Rouzina, I.; Bloomfield, V. A. *J. Mol. Biol.* **2000**, *296*, 1053−1063.

(3) Bronich, T.; Kabanov, A. V.; Marky, L. A. *J. Phys. Chem. B* **2001**, *105*, 6042−6050.

(4) Matulis, D.; Rouzina, I.; Bloomfield, V. A. *J. Am. Chem. Soc.* **2002**, *124*, 7331−7342.

(5) Pozharski, E.; MacDonald, R. C. *Biophys. J.* **2002**, *83*, 556−565.

(6) Keller, M.; Tagawa, T.; Preuss, M.; Miller, A. D. *Biochemistry* **2002**, *41*, 652−659.

(7) Keller M.; Jorgensen, M. R.; Perouzel, E.; Miller, A. D. *Biochemistry* **2003**, *42*, 6067−6077.

(8) Ehtezazi, T.; Rungsardthong, U.; Stolnik, S. *Langmuir* **2003**, *19*, 9387−9394.

(9) Rungsardthong, U.; Ehtezazi, T.; Bailey, L.; Armes, S. P.; Garnett, M. C.; Stolnik, S. *Biomacromolecules* **2003**, *4*, 683−690.

(10) Nisha, C. K.; Manorama, S. V. *Langmuir* **2004**, *20*, 2386-2396.

(11) Freire, E.; Mayorga, O. L.; Straume, M. *Anal. Chem.* **1990**, *62*, 950A-959A.

(12) ITC Data Analysis in Origin, Ver.5.0; MicroCal, Inc.: Studio City, CA, 1998; pp 73−78.

(13) (a) Oosawa, F. *Polyelectrolytes*; Marcel Dekker: New York, 1971. (b) Manning, G. S. *Q. Rev. Biophys.* **1978**, *11*, 179−246.

(14) Wilson, R. W.; Bloomfield, V. A. *Biochemistry* **1979**, *18*, 2192−2196.

(15) Yamasaki, Y.; Teramoto, Y.; Yoshikawa, K. *Biophys. J.* **2001**, *80*, 2823−2832.

(16) Teif, V. B.; Lando, D. Y. *Mol. Biol.* **2001**, *35*, 106−107.

(17) Mel'nikov, S. M.; Sergeyev, V. G.; Yoshikawa, K. *J. Am. Chem. Soc.* **1995**, *117*, 9951−9956.

(18) Bloomfield,V. A. *Curr. Opin. Struct. Biol.* **1996**, *6*, 334−341.

(19) Katayose, S.; Kataoka, K. *Bioconjugate Chem.* **1997**, *8*, 702−707.

(20) Harada A.; Kataoka K. *Macromolecules* **1995**, *28*, 5294−5299.

(21) Yamasaki, Y.; Katayose, S.; Kataoka, K.; Yoshikawa, K. *Macromolecules* **2003**, *36*, 6276−6279.

(22) Yoshikawa, K.; Kidoaki, S.; Takahashi, M.; Vasilevskaya, V. V.; Khokhlov, A. R. *Ber. Bunsen-Ges. Phys. Chem.* **1996**, *100*, 876−880.

(23) McGhee, J. D.; von Hippel, P. H. *J. Mol. Biol.* **1974**, *86*, 469−489.

(24) Schwarz, G. *Eur. J. Biochem.* **1970**, *12*, 442−453.

(25) Hud, N. V.; Downing, K. H.; Balhorn, R. *Proc. Natl. Acad. Sci. U.S.A.* **1995**, *92*, 3581−3585.

Knee Surg Sports Traumatol Arthrosc (2006) 14:1094–1100
DOI 10.1007/s00167-006-0129-3

KNEE

Long term results of anterior cruciate ligament reconstruction with iliotibial tract: 6-, 13-, and 24-year longitudinal follow-up

Satoshi Yamaguchi · Takahisa Sasho · Akihiro Tsuchiya · Yuichi Wada · Hideshige Moriya

Received: 16 November 2005 / Accepted: 13 February 2006 / Published online: 15 July 2006

Abstract Many studies have reported successful outcomes less than 10 years after anterior cruciate ligament (ACL) reconstruction. However, longer-term outcomes have not been analyzed. We assessd outcomes 24 years after anterior cruciate ligament reconstruction with iliotibial tract and compared them with shorter-term results in the same patients. Between 1979 and 1981, 45 patients underwent combined intra- and extra-articular ACL reconstruction with iliotibial tract. Follow-up evaluations of these patients were performed at 6, 13, and 24 years after surgery, which included manual and instrumental laxity testing, functional assessments, and radiography. Twenty-six (60%) patients of the original ACL reconstruction cohort participated in all three follow-up assessments. Three patients had undergone meniscectomy prior to ACL reconstruction and 18 underwent meniscectomy together with ACL reconstruction. Eleven patients underwent subsequent meniscectomy. The mean Lysholm score was 96.2, 93.8, and 87.8 at 6-, 13-, and 24-year follow-up, respectively. A significant decrease in mean Lysholm score was found between 13- and 24-year follow-up. The mean KT-1000 side-to-side difference was 3.5 mm at 24-year follow-up. Overall knee laxity did not change significantly during the follow-up period. At 24-year follow-up, 17 (71%) patients had moderate or severe degenerative changes on radiographs although about 50% of the patients participated in regular sports activities and no patient required regular clinical intervention.

Keywords ACL · Reconstruction · Long-term results · Iliotibial tract · Degenerative change

S. Yamaguchi · T. Sasho (✉) · H. Moriya
Department of Orthopaedic Surgery,
Graduate School of Medicine, Chiba University,
1-8-1 Inohana, Chuo-ku, Chiba 260-8677, Japan
e-mail: sasho@faculty.chiba-u.jp

A. Tsuchiya
Funabashi Orthopaedic Sports Medicine Center,
1-833 Hazama, Funabashi, Chiba 274-0822, Japan

Y. Wada
Department of Orthopaedic Surgery, Ichihara Hospital,
Teikyo University School of Medicine, 3426-3 Anesaki,
Ichihara, Chiba 299-0111, Japan

Introduction

Rupture of the anterior cruciate ligament (ACL) is one of the most common injuries in sports activities and more than 100,000 ACL injuries occur each year in young athletes in the United States [11]. In many cases, surgical reconstruction of the ligament is recommended, with the primary goal of surgery being restoration of knee stability. Many studies have reported successful short-term and intermediate-term results following ACL reconstruction [8, 14, 17, 31, 34]; however, longer-term outcomes have not been well studied. To our knowledge, only six studies have analyzed outcomes more than 10 years after surgery [6, 13, 18, 20, 25, 26]. Even longer follow-up periods should be evaluated, since most patients who undergo ACL reconstruction are young and remain active in sports for 15 or more years after surgery [2]. In addition, Shelbourne et al. [30] suggested that long-term follow-up should be performed consistently at 10, 15, and 20 years after ACL reconstruction because damage to

the knee joint does not appear to be affecting knee function until approximately 7 years after surgery.

In our hospital, ACL reconstruction with iliotibial tract (ITT) has been performed since 1979. The purpose of this study was to evaluate 24-year results after this technique and to compare them with those of 6- and 13-year follow-ups in the same patient cohort.

Materials and methods

Patients

Between 1979 and 1981, a total of 45 patients (32 males, 13 females) underwent ACL reconstruction in our hospital and an affiliated hospital. The mean age at surgery was 23.9 years (range 15–43 years). The mean interval from injury to surgery was 33.3 months (range 1–218 months). The follow-up, which consisted of physical examination and objective testing, was conducted three times at 6, 13 and 24 years after surgery. The present study includes only patients who completed all three follow-up visits.

Surgical technique

The surgical procedure consisted of intra- and extra-articular reconstruction with ITT. All surgeries were performed by two experienced orthopedic surgeons, including one senior author (HM).

A 25-cm longitudinal incision that dissected the subcutaneous tissue, was made on the lateral aspect of the thigh. A 2.5-cm-wide distally, 4-cm-wide proximally, and 22-cm-long strip of the ITT graft was harvested, leaving the tibial insertion (Gerdy's tubercle) attached. A 7.5-mm femoral hole was then drilled in an outside-in fashion. The entry point was 1 cm superior and 1 cm posterior to the origin of the fibular collateral ligament, and the intra-articular outlet was the superomedial corner of the lateral femoral condyle, just anterior to the joint capsule. A separate medial parapatellar incision was made. Thorough intra-articular pathology was investigated and meniscectomy was performed if necessary. A 7.5-mm tibial tunnel was drilled under direct vision from medial to the tibial tuberosity to the anterior half of the ACL stump. With forceps, the graft was passed deep to the fibular collateral ligament and through the femoral and tibial tunnels. With the knee at 90° flexion and the foot externally rotated, the graft was pulled taut and sutured to the fibular collateral ligament and the periosteum of the lateral femoral condyle. Then, with the knee at 30°flexion and the foot kept externally rotated, the graft was sutured to the periosteum around the outlet of the tibial tunnel (Fig. 1).

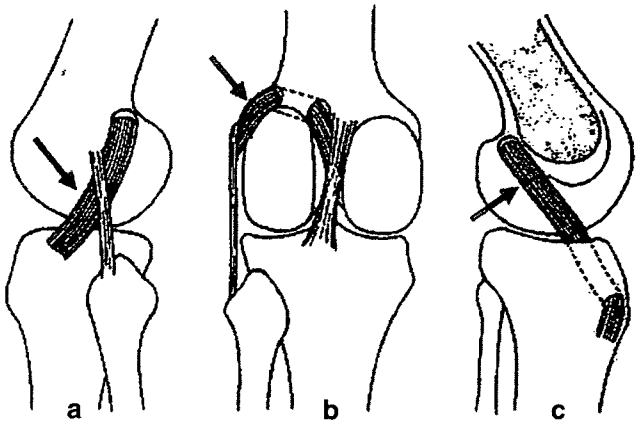

Fig. 1 Lateral (**a**), posterior (**b**), and intercondylar (**c**) views of a representative reconstructed ACL knee. *Arrows* show the ACL graft. Combined intra- and extra-articular reconstruction with iliotibial tract (ITT) was performed

Post operatively, a long leg cast allowing 30° flexion was applied for 4 weeks. A knee brace was used for a month thereafter. Partial weightbearing was allowed for 3 weeks with crutches after surgery and gradually increased as tolerated. Straight leg raising exercise was started the day after surgery, straight running was allowed after 3 months, and pivoting sports were allowed after 10 months, although this was individualized among patients.

Follow-up evaluations

Two orthopedic knee surgeons who were not involved in the surgery performed follow-up evaluations. One surgeon (AT) performed the 6- and 13-year follow-ups and the other (SY) performed the 24-year follow-up.

Pre- and postoperative knee function was assessed using the Lysholm score. A Lysholm score of 95–100 was graded as excellent, 84–94 as good, 65–83 as fair, and ≤82 as poor, according to the Tegner and Lysholm criteria [32]. Activity level was assessed using the Tegner activity score. The Tegner score was categorized as follows: level 0–3 corresponded to daily activities without any sports, 4–6 to recreational sports, and 7–10 to competitive sports, according to Andersson-Molina et al [2].

Postoperative laxity measurements were performed using the manual Lachman test and the KT-1000 arthrometer (MEDmetric, San Diego, California, USA). The Lachman test was performed at all follow-ups, and was graded as – or + at 6- and 13-year follow-up and as – to 3+ (according to IKDC grading) at 24-year follow-up, compared with the contralateral knee. The

KT-1000 arthrometer testing was performed at 13- and 24-year follow-up. Manual maximum side-to-side differences were recorded.

Radiographic assessment was performed at 24-year follow-up. Bilateral weightbearing radiographs were taken with the knee at 45 of flexion. The radiographs were graded as normal, nearly normal, abnormal, or severely abnormal according to IKDC grading.

Statistical analysis

The Wilcoxon single-rank tests were employed to examine the differences between each follow-up for the Lysholm score, the Tegner activity score, and the KT-1000 value. Spearman's rank correlation coefficients were used to examine the correlations between the Tegner activity score, the KT-1000 value, degenerative changes on radiographs, and the Lysholm score at 24-year follow-up. The level of statistical significance was set at $P < 0.05$.

Results

Follow-up

Despite extensive and exhaustive searches, 18 patients were lost to follow-up. Thirteen patients could not be located, three were contacted but could not return to our hospital for physical examinations due to geographic constraints, and two refused to participate in this study because they did not show any complaints. Of the remaining 27 patients, one patient had a revision ACL reconstruction with synthetic material 8 years after the first reconstruction because she injured her reconstructed ACL 1 year after the initial surgery. She was not included. Twenty-six patients (18 males, 8 females) were therefore included in the 24-year follow-up study. The right knee was involved in 14 patients and the left knee was involved in 12 patients. The mean age at surgery was 24.8 years (range, 16–42 years). The mean interval between injury and surgery was 42.5 months (range, 1–218 months). Six (23%) patients underwent surgery within 3 months after injury, 12 (15%) patients between 4 and 12 months, and 17 (62%) patients after more than 12 months. The most common causes of injury were soccer (35%), basketball (19%), and gymnastics (12%). Twenty-five (96%) patients were injured during sports participation.

Associated surgeries/injuries

Three patients had undergone surgeries prior to their reconstructions: one medial meniscectomy, one lateral meniscectomy (we could not obtain information whether they were partial or total meniscectomy), and one ACL suture. At the time of ACL reconstruction, associated procedures were performed in 18 patients: 15 underwent medial meniscectomy, one underwent lateral meniscectomy, and two underwent both medial and lateral meniscectomies. Two patients received medial collateral ligament repairs. After the reconstruction surgeries, additional surgeries were performed in 11 patients: five underwent medial meniscectomy, four underwent lateral meniscectomy, one underwent both medial and lateral meniscectomies. One experienced postoperative stiffness and underwent debridement of scar tissue, and also had lateral meniscectomy later. During the follow-up period, six patients (5 males, 1 female) sustained ACL injury of the contralateral knee.

Lysholm score

The mean Lysholm scores before surgery and at 6-, 13-, and 24-year follow-up were 63.6 (range 35–91), 96.2 (range 82–100), 93.8 (range 71–100), and 87.8 (range 71–100), respectively. Table 1 shows the Lysholm scores of all patients at each follow-up. At 6-year follow-up, one (4%) patient was graded as fair or poor. This number rose to two (8%) at 13-year follow-up and seven (27%) at 24-year follow-up.

Tegner activity score

The mean Tegner activity score before injury was 7.0 (range, 5–10). This decreased to 6.0 (range 3–9), 5.0

Table 1 Lysholm scores at each follow-up, ($n = 26$)

	Before op.	6-year ($P = 0.15$)	13-year ($P = 0.15$, $P < 0.001$)[a]	24-year ($P < 0.001$)[a]
Average ± SD	63.6 ± 13.4	96.2 ± 4.8	93.8 ± 7.7	87.8 ± 10.0
Excellent (95–100) (%)	0 (0%)	21 (81%)	17 (65%)	11 (42%)
Good (84–94)	1 (4%)	4 (15%)	7 (27%)	8 (31%)
Fair/poor (65–83/ < 64)	25 (96%)	1 (4%)	2 (8%)	7 (27%)

[a]Difference is statistically significant

Table 2 Tegner activity scores at each follow-up, (n = 26)

	Before injury	6-year (P= 0.002)[a]	13-year (P = 0.002, P = 0.003)[a]	24-year (P = 0.003)[a]
Average ± SD	7.0 ± 1.4	6.0 ± 1.5	5.0 ± 1.5	4.0 ± 1.6
7–10	14 (54%)	10 (38%)	6 (23%)	2 (8%)
4–6	2 (8%)	14 (54%)	16 (62%)	10 (38%)
0–3	0 (0%)	2 (8%)	4 (15%)	14 (54%)

[a]Difference is statistically significant

(range 2–7), and 4.0 (range 2–7) at 6-, 13-, and 24-year follow-up, respectively. Table 2 shows the Tegner scores for all patients at each follow-up. Although activity level decreased over time, 12 (46%) patients regularly participated in sports even at 24-year follow-up. The reasons for decrease in the activity as scored 3 or below were pain (3 patients), instability (4), decline in physical fitness (2), life style change (5). No correlation between the Lysholm and Tegner scores at 24-year follow-up was apparent (P = 0.33, rs = 0.19).

Laxity measurements

The 20 patients who did not sustain ACL injury on the contralateral knee were assessed for laxity measurements (Table 3). At 6-year follow-up, 10 (50%) patients had a negative Lachman test. At 13-year follow-up, two of these patients had a positive Lachman test due to traumatic re-injury of the reconstructed ACL. Two of the patients who had had a positive Lachman at 13-year follow-up had a negative at 24-year follow-up. At 24-year follow-up, 10 (50%) patients were graded as negative (–), five (25%) patients as +, three (15%) patients as 2+, and one patient (5%) as 3+.

The mean manual maximum side-to-side difference for the KT-1000 value was 4.0 mm (range, –1.5–14) at 13-year follow-up and 3.5 mm (range, –1.5–12.5) at 24-year follow-up. No significant difference was found between 13- and 24-year follow-up. At 24-year follow-up, four (20%) patients had a KT-1000 value >5 mm. A significant correlation was found between the KT-1000 value and the Lysholm score at 24-year follow-up (P = 0.01, rs = –0.59).

Table 3 Laxity measurements at each follow-up (n = 20)

	6-year	13-year (P = 0.20)	24-year (P = 0.20)
KT-1000			
Average ± SD	–	4.0 ± 3.1	3.5 ± 3.2
–1–2	–	8 (40%)	10 (50%)
3–5	–	9 (45%)	6 (30%)
6–9	–	2 (10%)	3 (15%)
10–	–	1 (5%)	1 (5%)
Lachman test			
–	10 (50%)	8 (40%)	10 (50%)
+	10 (50%)	12 (60%)	6 (30%)
2+	–	–	3 (15%)
3+	–	–	1 (5%)

Radiographic assessment

We were not able to obtain radiographs of two patients. Table 4 shows the distribution of IKDC grading on radiograph for these patients. On their operated knees, 17 (71%) patients were graded as abnormal or severely abnormal while only two (8%) patients were graded as normal. On the contralateral knees, 10 (42%) patients showed normal radiographic findings while four (17%) were graded as abnormal or severely abnormal. No correlation was found between radiographic grading and the Lysholm score at 24-year follow-up (p = 0.09, rs = –0.34). No patients required regular clinical intervention for either knee. Tables 5, 6 show correlations between degenerative change and meniscectomy in medial and lateral compartment. There was a tendency to develop degenerative changes in patients who underwent meniscectomy.

Discussion

Functional outcomes

In this study, we reported outcomes of ACL reconstruction 24 years after surgery. To our knowledge, this is the first study to evaluate outcomes more than 20 years after ACL reconstruction although six studies have reported results of more than 10 years [6, 13, 18,

Table 4 Degenerative changes on radiograph at 24-year follow-up (n = 24)

	Operated knee	Contralateral knee
Normal	2 (8%)	10 (42%)
Nearly normal	5 (21%)	10 (42%)
Abnormal	6 (25%)	2 (8%)
Severely abnormal	11 (46%)	2 (8%)

Table 5 Correlation between degenerative change at 24-year follow-up and meniscectomy in the medial compartment ($n = 24$)

	Total	Meniscectomy (+)	Meniscectomy (−)
Normal	3 (13%)	0	3
Nearly normal	7 (29%)	7	0
Abnormal	3 (13%)	3	0
Severely abnormal	11 (46%)	10	1

20, 25, 26]. In the present study, the mean Lysholm score was 93.8 and 87.8 at 13- and 24-year follow-up, respectively.

This study showed that the mean Lysholm score was 96.2, 93.8, and 87.8 at 6-, 13-, and 24-year follow-up, respectively. In addition, the proportion of patients who received a fair or poor Lysholm score increased from 8% at 13-year follow-up to 27% at 24-year follow-up, although no patients required regular clinical intervention. This indicates that the 13-year follow-up period was not long enough to evaluate long-term function after ACL reconstruction and that additional follow-up was necessary. Several studies have reported outcomes at longitudinal follow-up after ACL reconstruction [3, 7, 10, 13, 21, 26, 27, 29]. Bach et al. [3] showed that the KT-1000 comparative data, and the Tegner, Lysholm scores were nearly identical between 2–4-year follow-up and 5–9-year follow-up. In contrast, Brandsson et al. [7] reported in a prospective study that the mean Lysholm score decreased from 95 points at 2-year follow-up to 90 at 4–7-year follow-up. However, these studies assessed patients less than 10 years after surgery and they appear to need further follow-up research.

Degenerative changes

Previous papers have reported varying degrees of degenerative changes, from 3 [10] to 83% [20], following ACL reconstruction [10, 12, 18, 20, 21, 25, 28]. Seventy-one percent of the patients, in the present study, had moderate or severe degenerative changes on the operated knees while 17% showed degenerative changes on the contralateral knees at 24-year follow-up. Also an association between time from ACL injury to surgery and subsequent meniscus injury has been demonstrated by Daniel et al. [9]. In addition, an association between meniscectomy at ACL reconstruction and later degenerative changes has been well documented [1, 12, 21, 23, 24, 28]. For this reason, Jomha et al. [21] and other investigators [30] recommended early reconstruction to prevent degenerative changes after surgery. However, in the 1970s, diagnostic and treatment methods for ACL injury had not been well defined, so many ACL injuries might have been initially overlooked. Subsequently the mean time from injury to surgery was relatively long (42.5 months) and a subsequently high proportion (69%) of these patients underwent meniscectomy before and during the ACL reconstruction procedure.

Table 6 Correlation between degenerative change at 24-year follow-up and meniscectomy in the lateral compartment ($n = 24$)

	Total	Meniscectomy (+)	Meniscectomy (−)
Normal	8 (33%)	0	8
Nearly normal	6 (25%)	3	3
Abnormal	8 (33%)	5	3
Severely abnormal	2 (8%)	1	1

Among the high prevalence of degenerative changes, two patients were graded as normal. They underwent reconstruction surgery with meniscal preservation within 6 months after injury and their knees were stable even at 24 years. This suggests that modern ACL reconstruction techniques based on biomechanical and biomaterial analysis, which enable to re-establish a more stable knee, presumably have the possibility to give better long-term result than our series. This might also support Jomha's idea to reconstruct the ACL prior to the occurrence of secondary meniscal injuries [15, 21].

Surgical techniques and laxity

Currently, bone-patellar tendon-bone and hamstring tendons are the standard grafts for ACL reconstruction. However, ITT graft was widely used in the 1980s, and it has been the standard method in some clinics, particularly in Scandinavia [4]. Combined intra- and extra-articular reconstruction with ITT is thought to have several advantages over other types of grafts. For example, lateral tenodesis is believed to prevent excess pivoting [33]. In addition, ITT reconstruction does not disturb the extensor mechanism and reduces the risk of anterior knee pain [22]. Several studies [4, 5, 22] have reported excellent results following ACL reconstruction with ITT that are comparable to those with other grafts.

The surgical technique used in the present study involved some procedures that could affect postoperative knee stability; these are now considered to be inappropriate. First, the tibial tunnel was placed to the anterior half of the ACL stump, which is now considered too anterior because this could cause roof impingement [19] and laxity could develop. Second, the width of the ITT harvested for the ACL graft was

approximately 2.5 cm; this width does not provide sufficient strength for the ACL graft [29], and postoperative graft elongation could occur. Jorgensen et al. [22] also suggested that harvesting a 4- to 6-cm wide ITT graft was necessary. Actually, the mean side-to-side laxity was 3.5 mm and 20% of the patients had side-to-side laxity >5 mm at 24-year follow-up. The fact that as much as 11 (42%) patients underwent meniscectomy after the reconstruction surgery might also indicate that enough stability had not been restored in many patients, which is in contrast to the results of recent studies [7,14] that ACL reconstruction prevents subsequent meniscus injuries.

The KT-1000 side-to-side difference was correlated with Lysholm score at 24-year follow-up. This result contrasts with those of previous studies in which stability did not appear to be correlated with knee function [16, 29] in a short-term. But the effect of increased laxity should be followed for a long period even if short-term function is good, because knee function could deteriorate over time.

Limitation of this study

This study has many limitations. First, we were able to recruit only 26 (58%) out of 45 patients, which could affect the results. In addition, patients who undergo ACL reconstruction tend to be young and mobile, which make long term follow-up studies difficult. Second, this was a retrospective study with a limited patient population. Several studies have reported prospective results after ACL reconstruction with a large number of patients [7, 10]. However, only follow-ups of 10 years or less were reported in these studies. Third, we could not obtain enough data which could contribute the function and degenerative changes in radiographs including preoperative radiographs and cartilage status at the surgery.

Conclusion

The present study showed 24-year follow-up results after ACL reconstruction with ITT graft. Forty-two percent of the patients received an excellent Lysholm score and about 50% of the patients participated in regular sports activities in 24-year follow-up group, however overall function had deteriorated over time. The proportion of the patients who were graded as fair or poor increased from 8% in the 13-year follow-up to 27% in the 24-year follow-up. This indicates the necessity to follow-up patients for more than 20 years as well as the requirement of over 20 years period to know clinical benefits of ACL reconstruction.[7] Seventy-one percent of the patients had moderate or severe degenerative changes at 24-year follow-up although no patient required regular clinical intervention.

References

1. Aglietti P, Zaccherotti G, De Biase P, Taddei I (1994) A comparison between medial meniscus repair, partial meniscectomy, and normal meniscus in anterior cruciate ligament reconstructed knees. Clin Orthop Relat Res 307:165–173
2. Andersson-Molina H, Karlsson H, Rockborn P (2002) Arthroscopic partial and total meniscectomy. A long-term follow-up study with matched controls. Arthroscopy 18:183–189
3. Bach BR, Tradonsky S, Bojchuk J, Levy ME, Bush-Joseph CA et al (1998) Arthroscopically assisted anterior cruciate ligament reconstruction using patellar tendon autograft. Five- to nine-year follow-up evaluation. Am J Sports Med 26:202–209
4. Bak K, Jorgensen U, Ekstrand J, Scavenius M (1999) Reconstruction of anterior cruciate ligament deficient knees in soccer players with an iliotibial band autograft. A prospective study of 132 reconstructed knees followed for 4 (2–7) years. Scand. J Med Sci Sports 11:16–22
5. Bak K, Jorgensen U, Ekstrand J, Scavenius M (2001) Results of reconstruction of acute ruptures of the anterior cruciate ligament with an iliotibial band autograft. Knee Surg Sports Traumatol Arthrosc 7:111–117
6. Bonin N, Ait Si Selmi T, Donell ST, Dejour H, Neyret T (2004) Anterior cruciate reconstruction combined with valgus upper tibial osteotomy: 12 years follow-up. Knee 11:431–437
7. Brandsson S, Faxen E, Kartus J, Jerre R, Eriksson BI et al (2001) A prospective four- to seven-year follow-up after arthroscopic anterior cruciate ligament reconstruction. Scand J Med Sci Sports 11:23–27
8. Cain EL Jr, Clancy WG Jr (2002) Anatomic endoscopic anterior cruciate ligament reconstruction with patella tendon autograft. Orthop Clin North Am 33:717–725
9. Daniel DM, Stone ML, Dobson BE, Fithian DC, Rossman DJ et al (1994) Fate of the ACL-injured patient. A prospective outcome study. Am J Sports Med 22:632–644
10. Deehan DJ, Salmon LJ, Webb VJ, Davies A, Pinczewski LA (2000) Endoscopic reconstruction of the anterior cruciate ligament with an ipsilateral patellar tendon autograft. A prospective longitudinal five-year study. J Bone Joint Surg Br 82:984–991
11. Feagin JA Jr, Lambert KL, Cunningham RR, Anderson LM, Riegel J et al (1987) Consideration of the anterior cruciate ligament injury in skiing. Clin Orthop Relat Res 216:13–18
12. Ferretti A, Conteduca F, De Carli A, Fontana M, Matiani PP (1991) Osteoarthritis of the knee after ACL reconstruction. Int Orthop 15:367–371
13. Fink C, Hoser C, Hackl W, Navarro RA, Benedetto KP (2001) Long-term outcome of operative or nonoperative treatment of anterior cruciate ligament rupture—is sports activity a determining variable? Int J Sports Med 22:304–309
14. Freedman KB, D'Amato MJ, Nedeff DD, Kaz A, Bach BR (2003) Arthroscopic anterior cruciate ligament reconstruction: a meta analysis comparing patellar tendon and hamstring tendon autografts. Am J Sports Med 31:2–11